

The influence of the Atlantic Warm Pool on the Florida panhandle sea breeze

Vasubandhu Misra,^{1,2} Lauren Moeller,^{1,2} Lydia Stefanova,² Steven Chan,² James J. O'Brien,² Thomas J. Smith III,³ and Nathaniel Plant⁴

Received 21 November 2010; revised 25 April 2011; accepted 9 May 2011; published 4 August 2011.

[1] In this paper we examine the variations of the boreal summer season sea breeze circulation along the Florida panhandle coast from relatively high resolution (10 km) regional climate model integrations. The 23 year climatology (1979–2001) of the multidecadal dynamically downscaled simulations forced by the National Centers for Environmental Prediction–Department of Energy (NCEP-DOE) Reanalysis II at the lateral boundaries verify quite well with the observed climatology. The variations at diurnal and interannual time scales are also well simulated with respect to the observations. We show from composite analyses made from these downscaled simulations that sea breezes in northwestern Florida are associated with changes in the size of the Atlantic Warm Pool (AWP) on interannual time scales. In large AWP years when the North Atlantic Subtropical High becomes weaker and moves further eastward relative to the small AWP years, a large part of the southeast U.S. including Florida comes under the influence of relatively strong anomalous low-level northerly flow and large-scale subsidence consistent with the theory of the Sverdrup balance. This tends to suppress the diurnal convection over the Florida panhandle coast in large AWP years. This study is also an illustration of the benefit of dynamic downscaling in understanding the low-frequency variations of the sea breeze.

Citation: Misra, V., L. Moeller, L. Stefanova, S. Chan, J. J. O'Brien, T. J. Smith III, and N. Plant (2011), The influence of the Atlantic Warm Pool on the Florida panhandle sea breeze, *J. Geophys. Res.*, 116, D00Q06, doi:10.1029/2010JD015367.

1. Introduction

[2] Sea breeze is a regular feature of the summer season (June–July–August [JJA]) over Florida, especially over the Florida peninsula where there is usually a convergence of a double sea breeze front, one from the Atlantic coast and the other from the Gulf coast [*Blanchard and Lopez*, 1985]. Sea breeze fronts are typically forced by the temperature contrast between the warm land and the relatively cold ocean surface, creating a pressure gradient toward the land surface during daytime, which reverses at nighttime. *Anthes* [1978], using a 2-D mesoscale model, showed that the balance between the solenoidal term, the vertical diffusion of momentum, and the Coriolis force dominated the simulated sea breeze circulation.

[3] These sea breeze circulations and the consequent rainfall from it are typical mesoscale events, which are often not clearly captured in coarsely defined gridded observations. Here, we examine the variability of the sea breeze over Florida from a relatively high resolution (~10 km) regional climate model simulation.

[4] In an observational study, *Blanchard and Lopez* [1985] have characterized the south Florida sea breeze into 4 types based on their inland penetration and sea breeze intensity. They suggest that these sea breeze variations exist as a result of the background synoptic conditions. Similarly, *Nicholls et al.* [1991] from their modeling study conclude that sea breeze characteristics are related to the prevailing wind speed and direction. In this paper we propose that the large-scale variations of winds and temperature forced by the variability in the Atlantic warm pool [*Wang and Enfield*, 2001; *Wang et al.*, 2006] have the potential to influence the sea breeze along the Florida coasts.

[5] For 1979–2001 we isolated 5 large and 5 small Atlantic Warm Pool (AWP) years, whose area of the AWP (enclosed by the 28.5° isotherm) in JJA was 1 standard deviation above and below the corresponding climatology, respectively. The average sea surface temperature (SST) [*Smith et al.*, 2008] and 850 hPa winds from the National Centers for Environmental Prediction–Department of Energy (NCEP-DOE) Reanalysis II (also referred to as R2)

¹Department of Earth, Ocean and Atmospheric Science, Florida State University, Tallahassee, Florida, USA.

²Center for Ocean-Atmospheric Prediction Studies, Florida State University, Tallahassee, Florida, USA.

³Southeast Ecological Science Center, U. S. Geological Survey, St. Petersburg, Florida, USA.

⁴St. Petersburg Coastal and Marine Science Center, U. S. Geological Survey, St. Petersburg, Florida, USA.

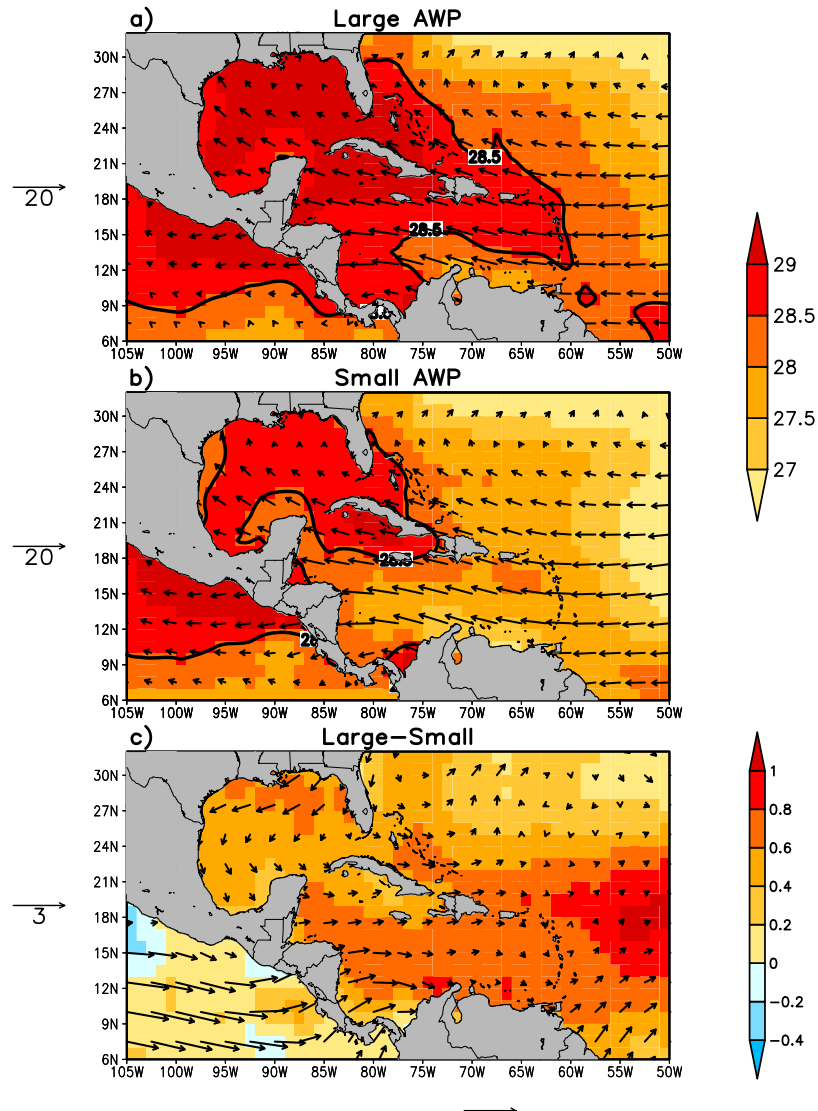


Figure 1. The JJA average SST ($^{\circ}\text{C}$) from ERSSTV3 [Smith *et al.*, 2008] and corresponding 850 hPa winds (m s^{-1}) from NCEP-DOE reanalysis [Kanamitsu *et al.*, 2002] for five (a) large (1981, 1987, 1995, 1998, 1999) and (b) small (1984, 1986, 1989, 1993, 1994) AWP years.

[Kanamitsu *et al.*, 2002] for the 5 large and 5 small AWP years are shown in Figures 1a and 1b, respectively. In years of large AWP, the trade winds are relatively weak [Wang and Enfield, 2003; Wang *et al.*, 2006] (Figure 1c), the Caribbean Low Level Jet (CLLJ) is also weak [Wang *et al.*, 2007; Chan *et al.*, 2010], evaporation from the ocean surface is weak [Misra *et al.*, 2009], and there is an increased cloud radiative feedback resulting in decreased longwave radiative loss [Wang and Enfield, 2001]. All of these lead to warmer temperatures of the ocean surface (Figure 1c). An estimate of the composite mean difference of the JJA seasonal mean rainfall from observations between these large and small AWP years (Figure 2), shows that the largest negative differences are found in the panhandle of Florida, followed by central and south Florida. In large AWP years, these regions of Florida have less summer seasonal rainfall than in small AWP years (Figure 2c). We contend in this

paper that these differences of seasonal mean rainfall especially along the northwestern coast of Florida are related to corresponding changes in the sea breeze circulation forced by the AWP variations.

[6] In the next section we describe the regional climate model used in this study and provide details of the conducted model experiments. The results are presented in section 3 followed by a discussion in section 4. The concluding remarks are included in section 4.

2. Model and Experiment Description

[7] The high-resolution atmospheric fields in the study are generated by downscaling the R2 using the NCEP-Experimental Climate Prediction Center (ECPC) regional spectral model (RSM) [Juang and Kanamitsu, 1994; Kanamitsu *et al.*, 2002]. In this downscaling procedure, every 6 h the R2

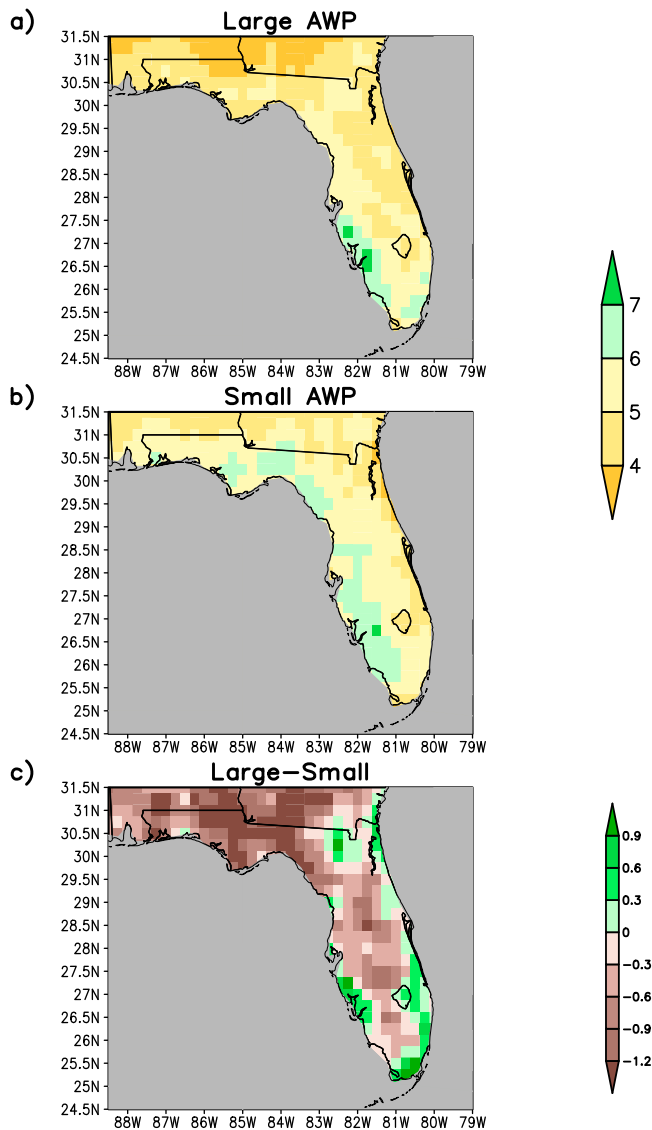


Figure 2. The JJA averaged CPC rain gauge based precipitation [Higgins *et al.*, 2000] for the (a) five large AWP years (from Figure 1), (b) five small AWP years (from Figure 2), and (c) difference of Figures 2a–2b. The units are in mm d^{-1} .

fields of atmospheric winds, temperature, humidity and surface pressure are imposed as lateral boundary conditions to the regional model integration. In the interior of the regional domain, scale-selective bias correction [Kanamaru and Kanamitsu, 2007] is used to reduce the large-scale error growth. The RSM is a Fourier-based spectral model using the primitive equations system under the hydrostatic assumption. The model configuration used in this study, including the physical parameterization schemes, is summarized in Table 1.

[8] The regional downscaling of R2 has been carried out from 1979 to 2001 and hereafter referred as RSM-R2. The SST used to force this model integration is the National Oceanic and Atmospheric Administration (NOAA) Extended

Reconstruction Sea Surface Temperature analysis version 3 (ERSSTV 3) [Smith *et al.*, 2008]. A previous study [Lim *et al.*, 2010] of summertime precipitation over the same domain demonstrated that downscaling the R2 with the RSM at 20 km resolution reduces the bias of the global reanalysis and produces realistic distribution of summer precipitation. That study also demonstrated that spatial patterns of wet versus dry years were successfully simulated in the downscaling.

[9] For the verification of the RSM-R2 we use the winds from the R2 analysis and precipitation from the unified daily U.S. precipitation analysis of the Climate Prediction Center (CPC) [Higgins *et al.*, 2000]. The CPC precipitation analysis is available at a $0.25^\circ \times 0.25^\circ$ grid resolution. In addition, the diurnal variability of precipitation is validated against the NCEP/Environmental Modeling Center (EMC) U.S. gridded multisensor estimated hourly precipitation analysis at 4 km grid resolution [Lin and Mitchell, 2005]. This data set is however available only for the period from 2002 to the present, which unfortunately does not overlap with the RSM-R2 integration period. However, we use this observed rainfall data set to validate the climatological diurnal variability of the rainfall.

3. Results

3.1. Climatology of the Diurnal Variability Over Florida

[10] One of the motivating factors for examining the seabreeze variation in the RSM-R2 is its reasonably good simulation of the diurnal variability of the rainfall over Florida (Figures 3 and 4). The observations (Figure 3) indicate that the observed climatological rainfall peaks at 16:00 EST over most of Florida. The RSM-R2 picks this observed feature reasonably well including the growth to this diurnal peak at approximately 13:00 EST over the South and parts of the Gulf coasts of Florida. Similarly, the observed slower demise of this diurnal peak in rainfall over South Florida with persistent higher-than-daily average rain rates at around 19:00 EST in contrast to the observed relative abrupt decrease in rainfall over the same 3 h period over northwestern Florida is also well captured by the RSM-R2

Table 1. A Brief Outline of the Regional Spectral Model

Model Feature	Description
Resolution	10 km horizontal resolution, 28 vertical terrain following sigma levels
Domain	$\sim 23^\circ\text{S}$ to 37.5°N and 98°W to 75°W
Topography	30 min USGS topography
Vegetation map	USGS converted to 12 NOAH vegetation types [Loveland <i>et al.</i> , 1995]
Land surface scheme	NOAH with 4 soil levels [Ek <i>et al.</i> , 2003]
PBL scheme	Nonlocal; [Hong and Pan, 1996]
Radiation Scheme	Chou and Lee [1996]; Chou and Suarez [1994]
Cloud water scheme	Diagnosed from relative humidity; Slingo [1987]
Convection scheme	Simplified Arakawa Schubert Scheme; (H.-L. Pan and W.-S. Wu, 1995) ^a

^aH.-L. Pan and W.-S. Wu, Implementing a mass-flux convective parameterization package for the NMC Medium Range Forecast Model, paper presented at 10th Conference on Numerical Weather Prediction, American Meteorological Society, Portland, Oregon, 1995).

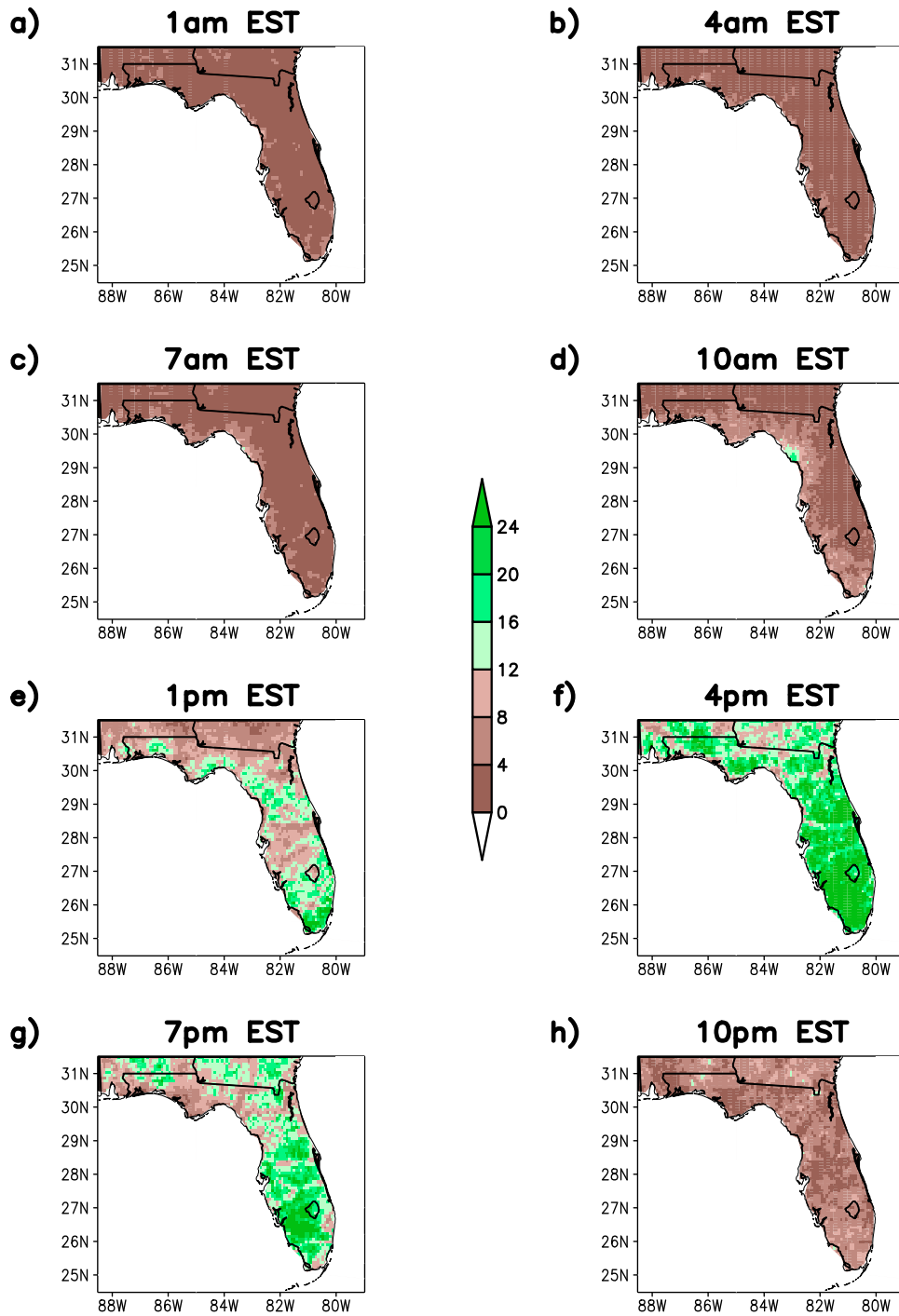


Figure 3. Observed climatology of summer season (June–July–August) rainfall based on multisensor precipitation analysis of *Lin and Mitchell* [2005] at 3 h interval. The climatology was computed for the available period of these observations, which is from 2002 to 2008. The units are in mm d^{-1} .

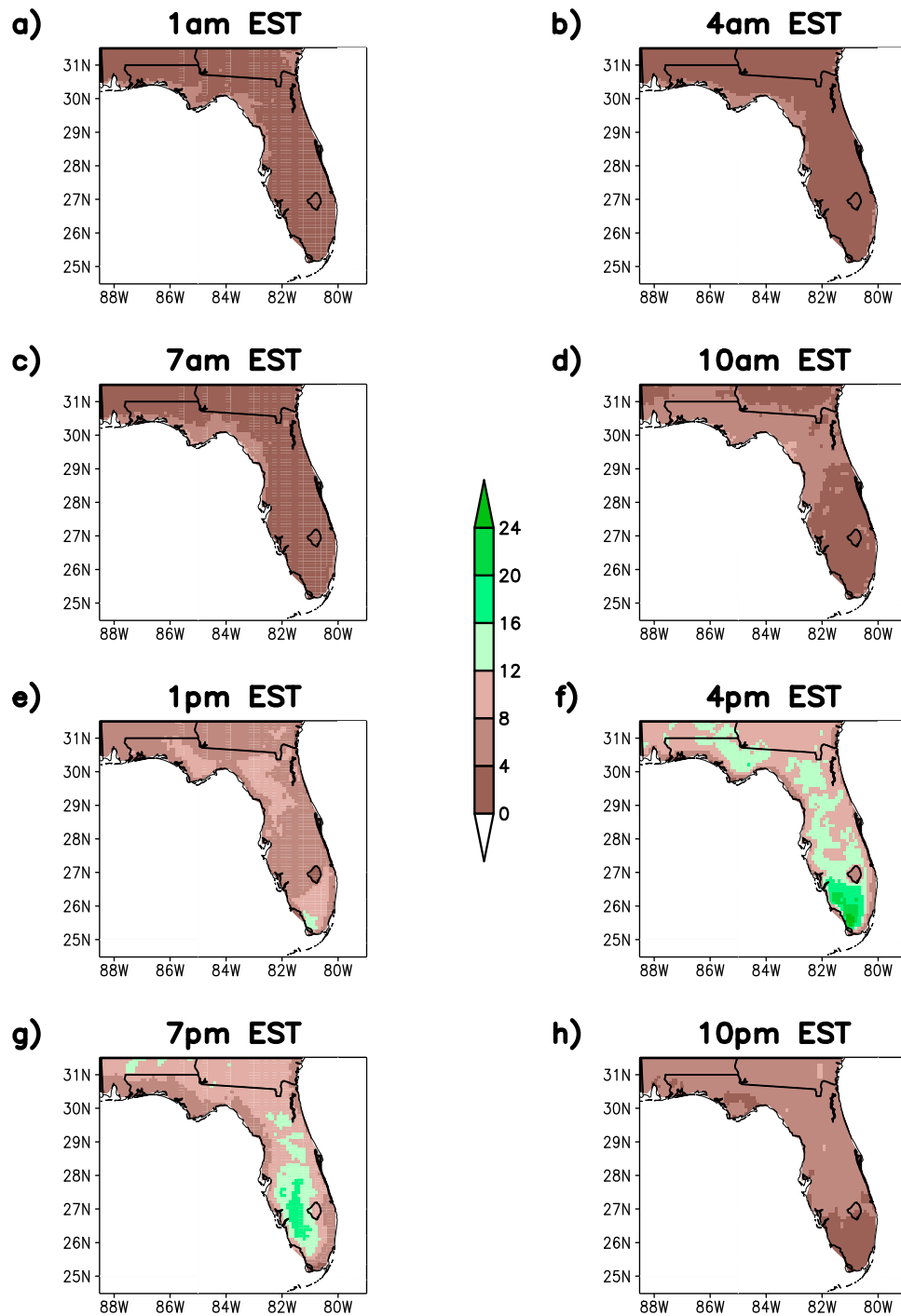


Figure 4. Same as Figure 3 but from RSM-R2 model simulation. The climatology was however computed from 1979 to 2001.

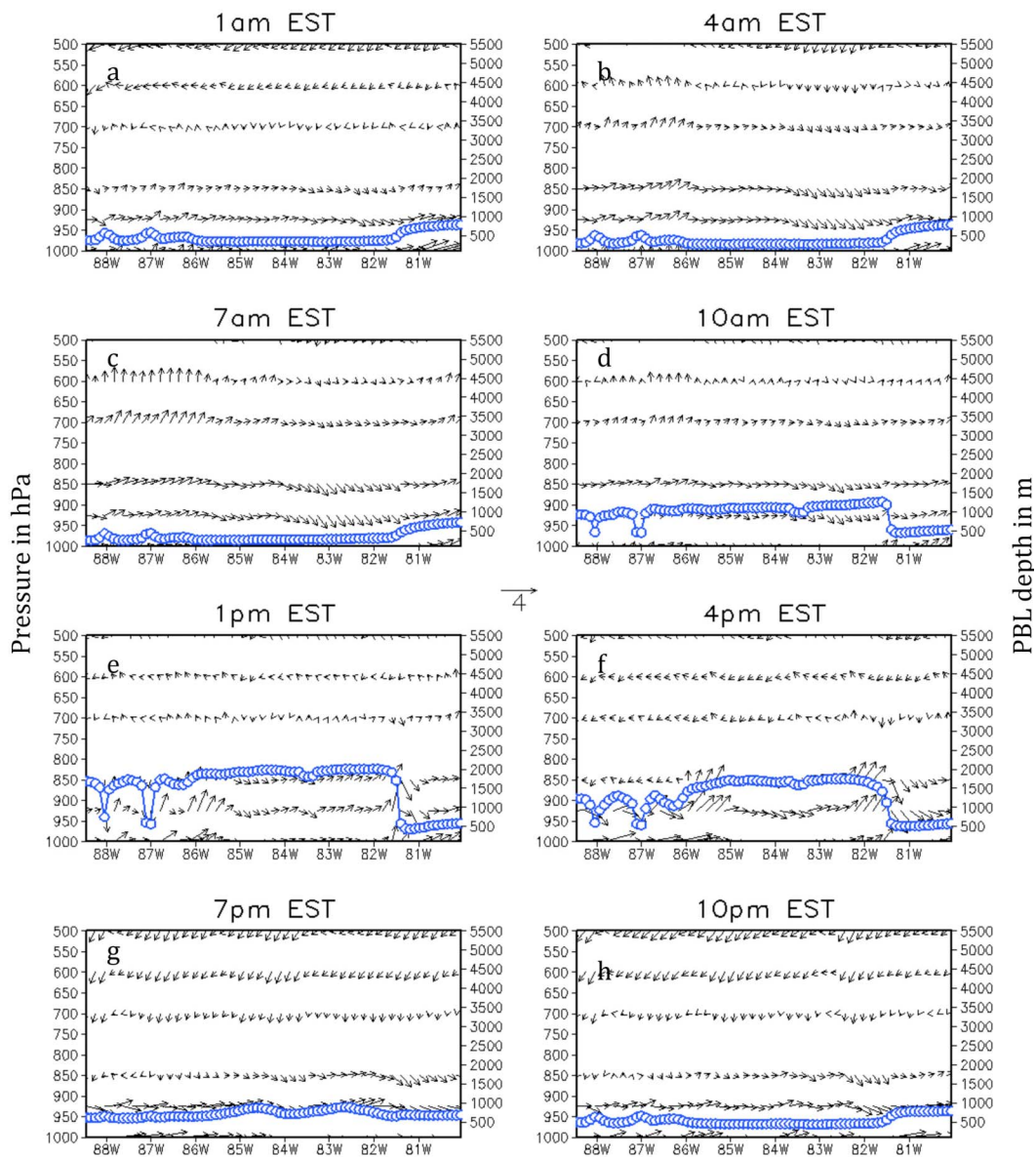


Figure 5. Cross section of the climatological June–July–August vertical circulation (vertical velocity and, meridional wind in m s^{-1}) at 30.5°N latitude, across south Florida at 3 hourly interval. The PBL height is shown by solid line with open circles. The vertical velocity is scaled by a factor of 100. Here arrows from left to right (right to left) are southerlies (northerlies).

integration. The phase of this diurnal variation of rainfall in south Florida is consistent with the observed analysis based on radar composites of *Blanchard and Lopez* [1985]. The RSM-R2 has an apparent bias of underestimation of the rain rates relative to the observations (Figure 3). However, it is a feature of the NCEP/EMC U.S. gridded multisensor estimated rainfall that while the timing of its diurnal phase change is reliable, the rainfall amounts have a wet bias (P. Xie, National Centers for Environmental Prediction, personal communication, 2010).

[11] We show the climatological vertical circulation and planetary boundary layer (PBL) height variations at these

diurnal scales through a vertical cross sections along 30.5°N (northwestern Gulf coast of Florida) from the RSM-R2 simulation in Figure 5. At this latitude, the longitudes of interest where the seabreeze effect will be most prominent are approximately 88°W to 84°W in Figure 5. As the diurnal peak in rainfall is reached at 16:00 EST (Figure 4) the height of the PBL diminishes from its peak at 13:00 EST (Figure 5e). This is a result of the strong mixing initiated by the breakout of the convection, evident from the sustained amplification of the vertical motions through 16:00 EST (Figure 5f). By 19:00 EST there is rapid weakening of the boundary layer circulation and a decrease in the PBL height

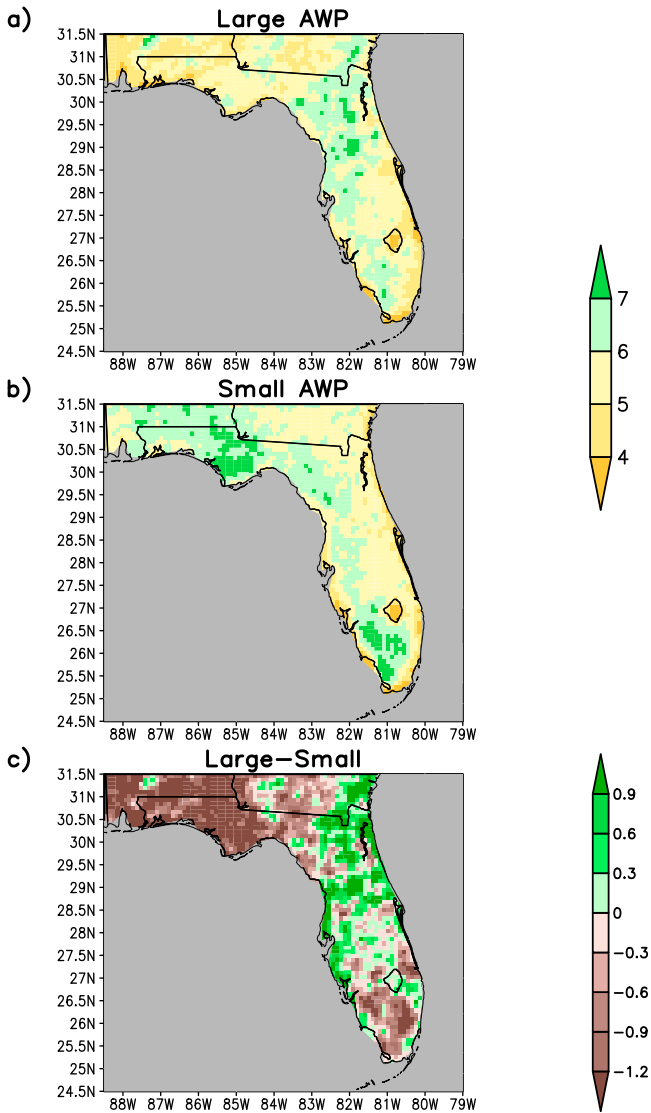


Figure 6. Same as Figure 2 but from RSM-R2 simulation.

along the northwestern Gulf coast of Florida (Figures 5g). This reduction in the intensity of the boundary layer circulation is also evident in the reduction of the rainfall from 16:00 (Figure 4f) to 19:00 (Figure 4g). The growth of the PBL is relatively gradual and continuous from its diurnal minimum at 04:00 EST. Therefore it may be noted that the diurnal variations of the PBL height and the circulation (Figure 5) are consistent with our results for rainfall (Figure 4).

3.2. Interannual Variability

[12] The composite average rainfall for the 5 large and the 5 small AWP years from the RSM-R2 simulation (Figures 6a and 6b) does a fair job in simulating the differences between the composites (Figure 6c) relative to the observations (Figure 2c). The spatial pattern of the rainfall (Figures 6a and 6b) and the differences (Figure 6c) are reasonable compared to the corresponding observations

(Figure 2). However, the magnitude of the differences in Figure 6c is clearly underestimated compared to the observations in Figure 2c. Furthermore, the drying anomaly in large AWP years in central Florida in Figure 6c is very poorly simulated compared to observations (Figure 2c).

[13] The composite continental surface air temperature and SST for large, small AWP years and their difference are shown in Figures 7a, 7b, and 7c, respectively. It is clear that in large AWP years the land becomes uniformly warmer than in small AWP years resulting in slightly stronger temperature gradients between the land and the neighboring ocean surface.

3.3. Interannual Variability of Diurnal Variations

[14] The composite mean difference of rainfall at intervals of 3 h between the large and the small AWP years from the RSM-R2 simulation (Figure 8), over the northwest coast of the Florida panhandle indicates a tendency for the differ-

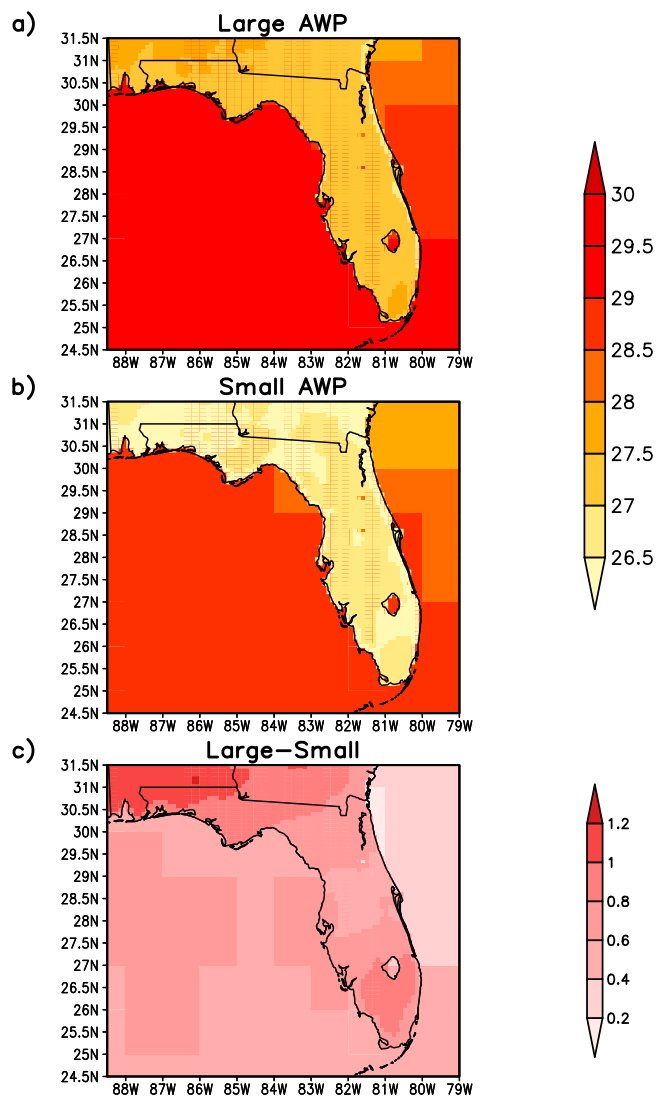


Figure 7. Same as Figure 2 but for land surface air temperature from RSM-R2 simulation and SST from observations. The units are in °C.

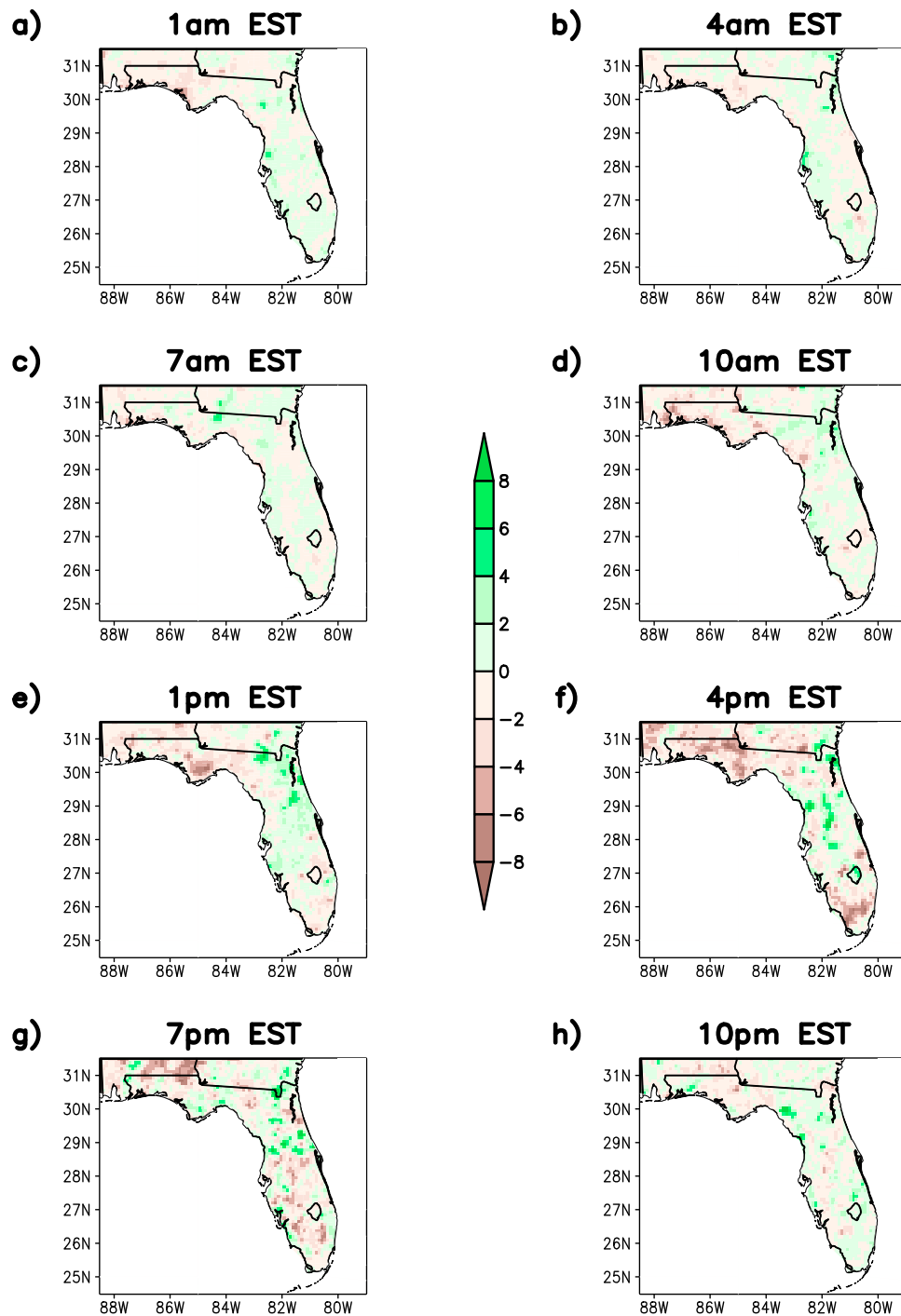


Figure 8. The JJA composite mean difference of rainfall between the five large and the five small AWP years shown at intervals of 3 h. The units are in mm d^{-1} . Here arrows from left to right (right to left) are southerlies (northerlies).

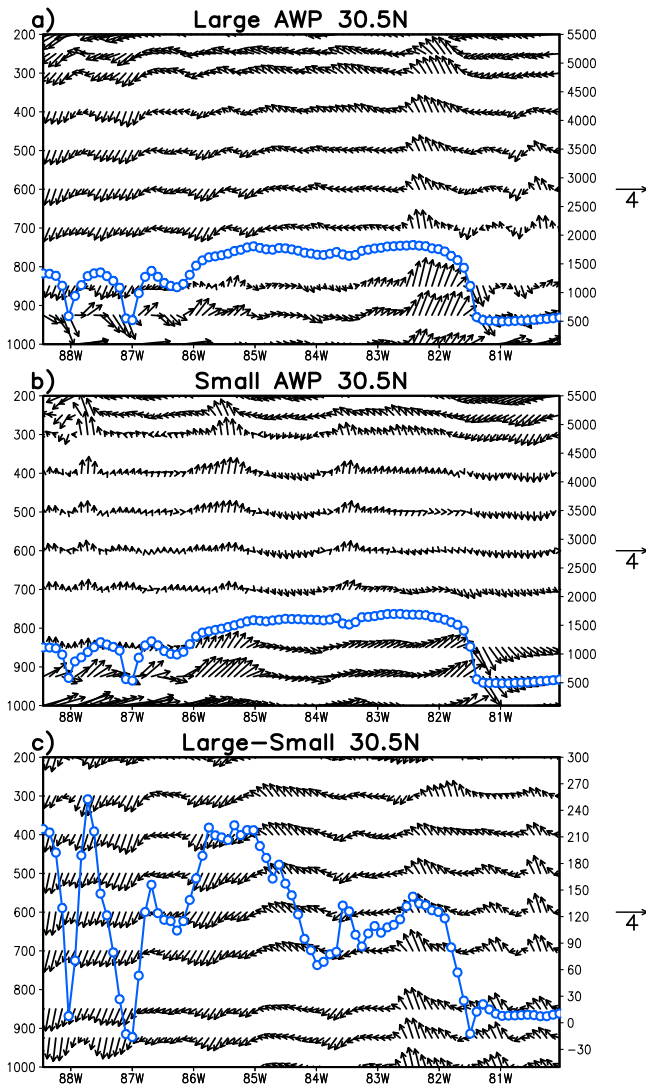


Figure 9. The JJA composite mean of PBL height (m) and vertical circulation (vertical velocity scaled by a factor of 100 and meridional wind) at 30.5°N for the (a) five large AWP years, (b) five small AWP years, and (c) the difference of Figures 9a and 9b from the RSM-R2 simulation at 16:00 EST. Here arrows from left to right (right to left) are southerlies (northerlies).

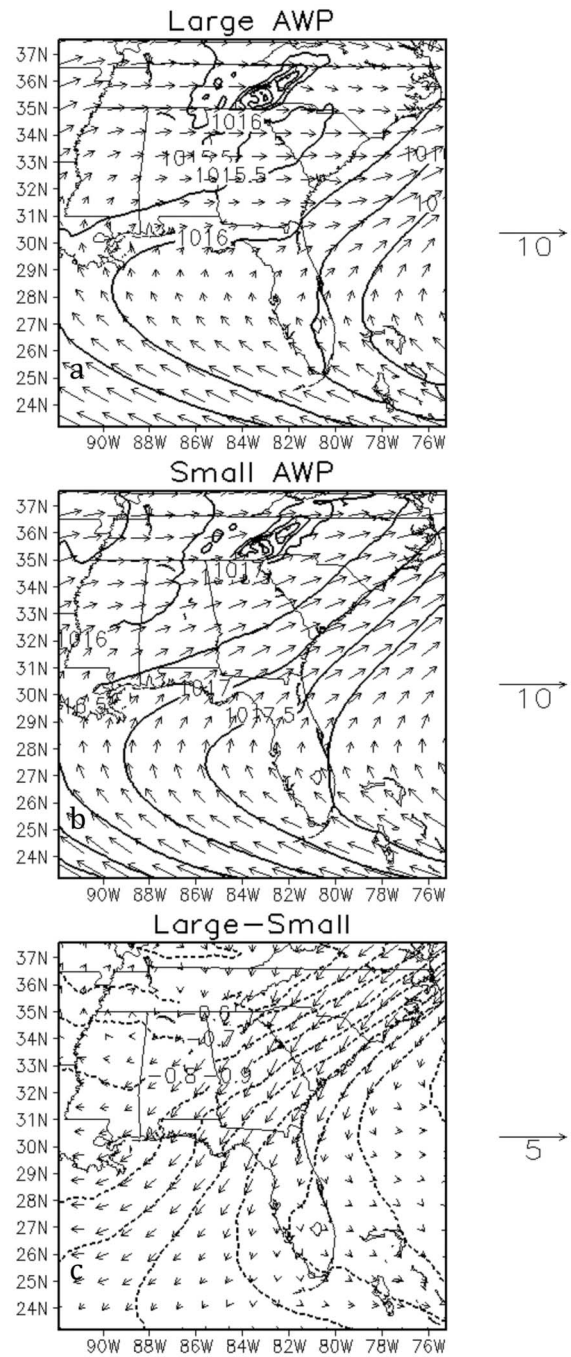


Figure 10. The JJA composite 850 hPa winds ($m s^{-1}$; scale is shown on the right of each panel) and mean sea level pressure in hPa (with contour interval of 0.5 hPa) for (a) large, (b) small, and (c) large-small AWP years.

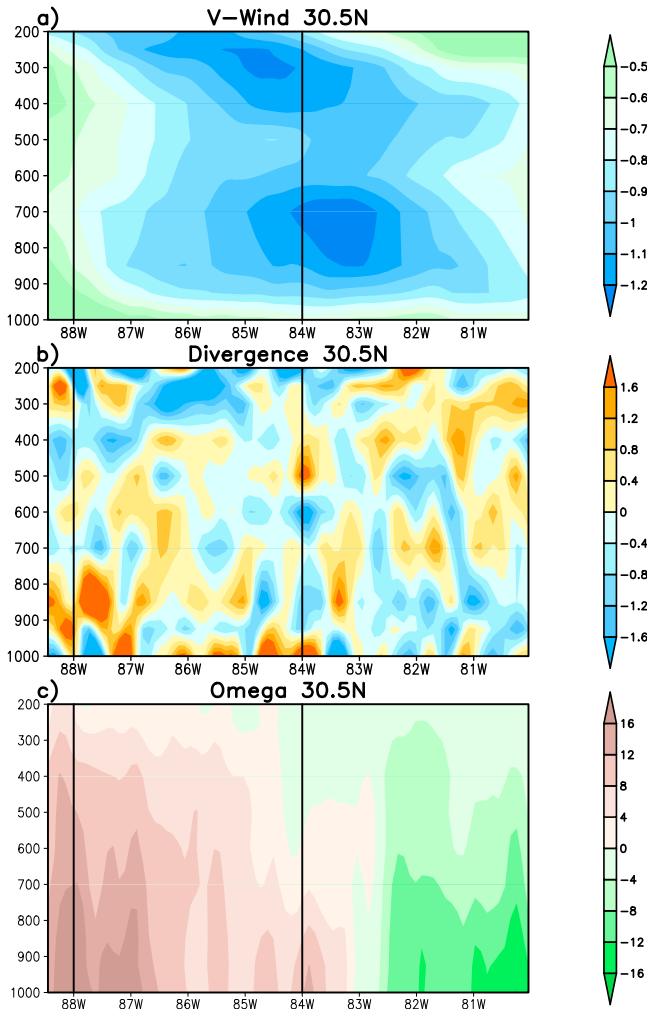


Figure 11. The JJA composite mean difference of (a) meridional wind (m s^{-1}), (b) divergence ($\text{X}10^6\text{s}^{-1}$), and (c) omega (vertical velocity, hPa s^{-1}) between large and small AWP years. The two vertical lines at 88W and 84W depict the boundaries of the panhandle Florida where the Sverdrup balance is best depicted in RSM-R2.

ences to be largest at the time of the climatological diurnal peak, namely at 16:00 EST. This result points to potential modulation of the sea breeze circulation at interannual time scales.

[15] The composite vertical cross section of the PBL height and circulation at 30.5°N at 16:00 EST for large and small AWP years and their difference are shown in Figures 9a, 9b, and 9c, respectively. The seabreeze circulation in the panhandle coast of Florida is weaker in large AWP years compared to small AWP years. However, it may be noted that the surface temperature contrasts between the land and ocean are stronger in large AWP years.

4. Discussion

[16] What is causing this interannual variability of rainfall in the summer season to peak at 16:00 EST over southwestern Florida and northwestern Florida in the RSM-R2

simulation? Our answer to this question lies in the modulation of the sea breeze circulation by the large-scale circulation. To further elaborate on this question, consider the composite mean differences of the 850 hPa winds and mean sea level pressure between the large and the small AWP years (Figure 10). In large AWP years the North Atlantic Subtropical High (NASH) is weaker (Figure 10a) compared to small AWP years (Figure 10b), resulting in a southward flow anomaly (Figure 10c). This is consistent with similar observations made in *Wang and Enfield [2003]* and *Wang et al. [2006]*. The anomalous northerlies in large AWP years are associated with the Sverdrup balance [*Rodwell and Hoskins, 2001; Hoskins and Wang, 2005*] given by

$$\beta V \approx f \frac{\partial \omega}{\partial p}, \quad (1)$$

where β is the meridional variation of the Coriolis parameter, f , V is the meridional wind and ω is the vertical velocity on pressure surface. Given the location of the panhandle region in the subtropics and its proximity to NASH, the Sverdrup balance applies quite well to the situation. In accordance with this balance the strong anomalous northerlies at the low level should be compensated by divergence and seen below the maximum anomalous descent. This feature is well captured in the RSM-R2 simulation. Figure 11 shows the vertical cross section along 30.5°N of the composite mean difference of the meridional wind (Figure 11a), divergence ($\frac{\partial \omega}{\partial p}$; Figure 11b), and vertical velocity (ω ; Figure 11c). The anomalous sinking motion in Figure 11c is consistent with an overall anomalous low-level (upper level) divergence (convergence) (Figure 11b; albeit a noisy field) in the panhandle region. Following the Sverdrup balance (equation 1) and mass continuity there is a large-scale anomalous sinking motion associated with low-level anomalous northerly flow along the panhandle coast of Florida in large AWP years compared to small AWP years. This anomalous northerly flow along the panhandle Florida is from the weakening of the NASH and its eastward movement in large AWP years relative to small AWP years as illustrated in the schematic in Figure 12. Consequently, this modulation of the large-scale flow makes the boundary layer circulation associated with the sea breeze weaker (Figures 10c and 12a) despite stronger land-ocean contrasts in large AWP years (Figure 7c).

[17] We examined the moisture budget at the diurnal peak of 16:00 EST (which also coincides with the peak in interannual variation seen in Figure 8) to further understand the low-frequency variations of the Florida sea breeze along the panhandle coast. The terms of the moisture budget equation follow from

$$\frac{\partial Q}{\partial t} = \underbrace{-\nabla \cdot M}_{\text{Term1}} + \underbrace{E}_{\text{Term3}} - \underbrace{P}_{\text{Term4}}, \quad (2)$$

where term 1 is time tendency of precipitable water, term 2 ($-\nabla \cdot M$) is moisture flux convergence (if positive) or moisture flux divergence (if negative), E is evaporation (term 3)

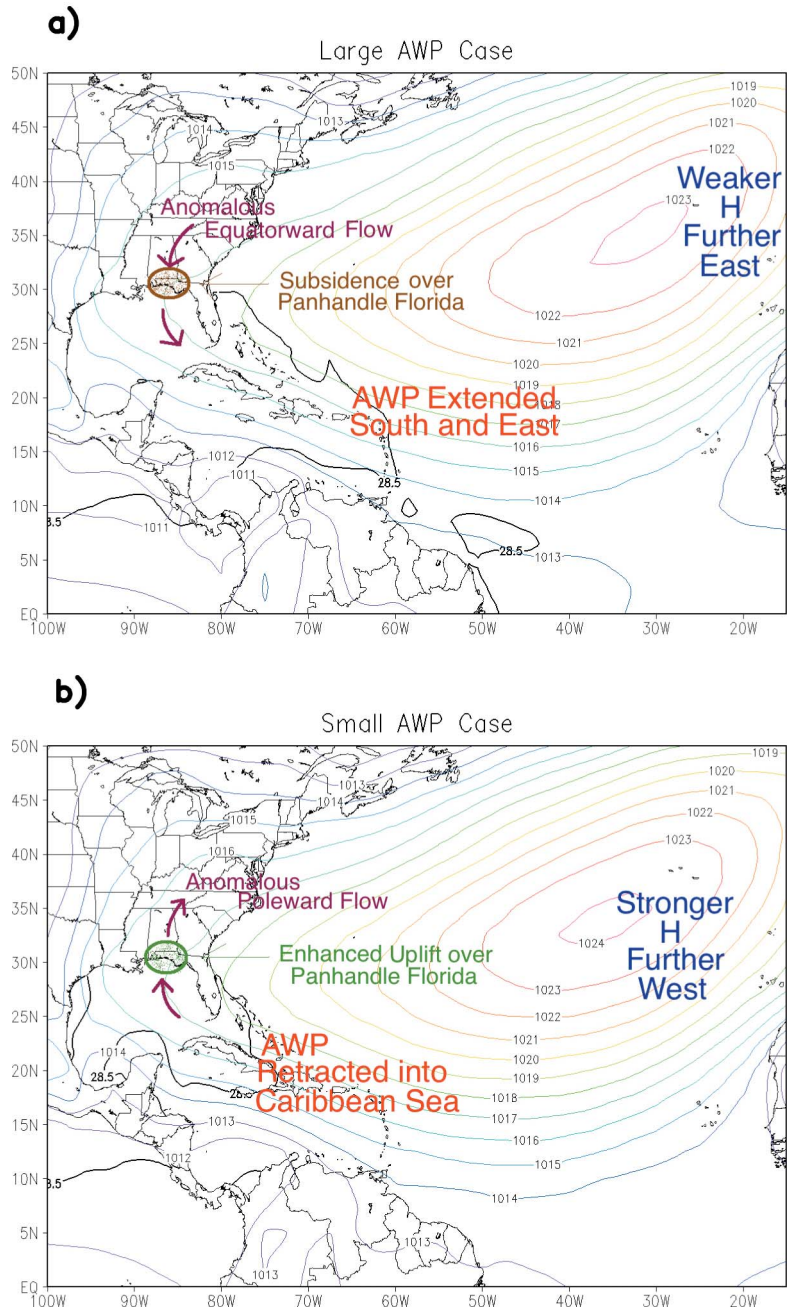


Figure 12. Schematic of the anomalous conditions over panhandle Florida generated by the modulation of the North Atlantic Subtropical High (NASH) in the (a) large and (b) small AWP years. The composite mean sea level pressure (hPa) from R2 is contoured for the five large (Figure 12a) and small (Figure 12b) AWP years.

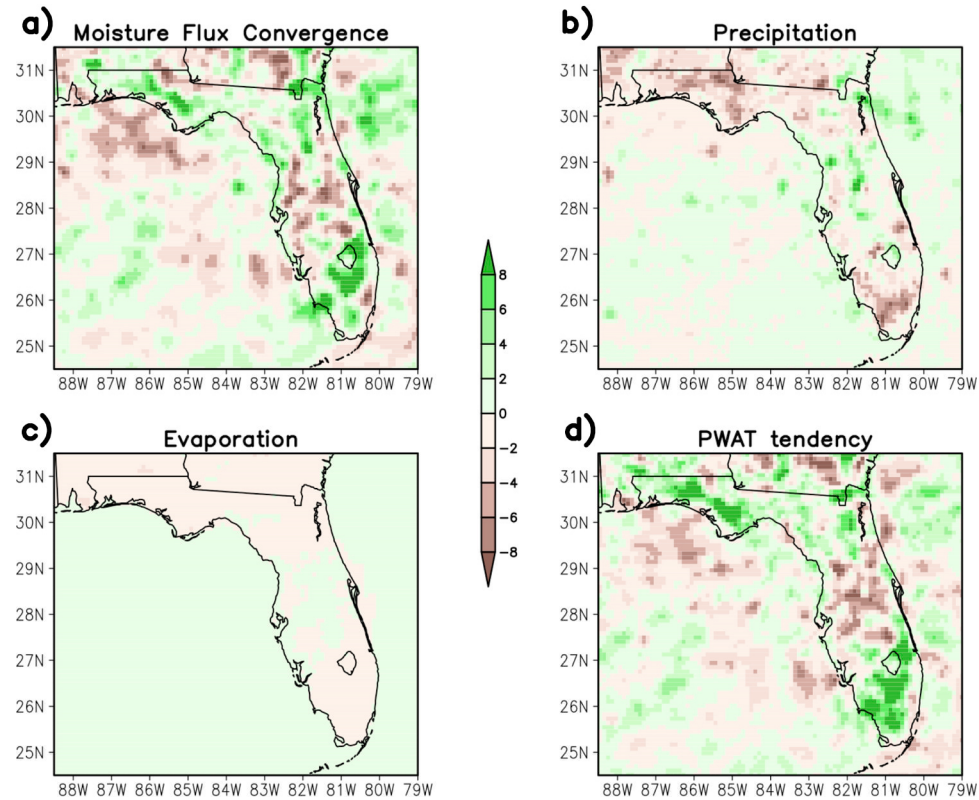


Figure 13. The JJA composite mean difference between the five large AWP and the five small AWP years at 16:00 EST of the (a) moisture flux convergence, (b) precipitation, (c) evaporation, and (d) tendency of precipitable water. The units of all variables are in mm d^{-1} .

and P is precipitation (term 4). The precipitable water (Q) and the moisture flux (M) are defined as,

$$Q = \frac{1}{g} \int_{p_s}^{200\text{mb}} q dp \quad \text{and} \quad M = \frac{1}{g} \int_{p_s}^{200\text{mb}} \vec{v} q dp.$$

[18] In the composite mean difference of the terms of the moisture budget at the climatological diurnal peak of 16:00 E.S.T from the RSM-R2 simulation we notice that the moisture flux convergence is slightly stronger in large AWP years compared to the small AWP years (Figure 13a). However, due to the unfavorable large-scale conditions from the displacement and weakening of the North Atlantic Subtropical High during large AWP years, the sea breeze convection is relatively suppressed (Figure 13b). Evaporation (Figure 13c) does not play as significant a role as the other terms of the moisture budget along the panhandle coast of Florida. There is therefore a compensatory decrease of the tendency of the precipitable water (Figure 13d) in large AWP years. This compensatory decrease in the tendency of the precipitable water in large AWP years, in fact, translates to higher precipitable water in the atmospheric column at 16:00 EST (Figure 14).

[19] The modulation of the small-scale diurnal variations of the sea breeze from the large-scale variations of the atmosphere and SST points to the importance of examining high-resolution data sets both from observations and models to understand climate variations along the coastlines of Florida.

5. Conclusions

[20] We have conducted a modeling study to understand the interannual variations of the summer seasonal rainfall over northwest Florida. Relatively high (10 km grid) resolution regional climate integrations were conducted for a period of 23 years from 1979 to 2001 forced with NCEP-DOE reanalysis at the lateral boundaries. This regional climate simulation showed reasonable skill in simulating the diurnal and interannual time scales of precipitation, when compared with observations. The observed diurnal peak and minimum of rainfall at 16:00 EST and 04:00 EST along Florida coasts are very well captured by the regional climate model integration RSM-R2.

[21] We also showed, that in years of large AWP, when the area enclosed by the 28.5°C isotherm over the general area of the Caribbean Sea, Gulf of Mexico, and northwest Atlantic is larger than normal with accompanying eastward shift and weakening of the North Atlantic Subtropical High, the sea breeze circulation and the associated con-

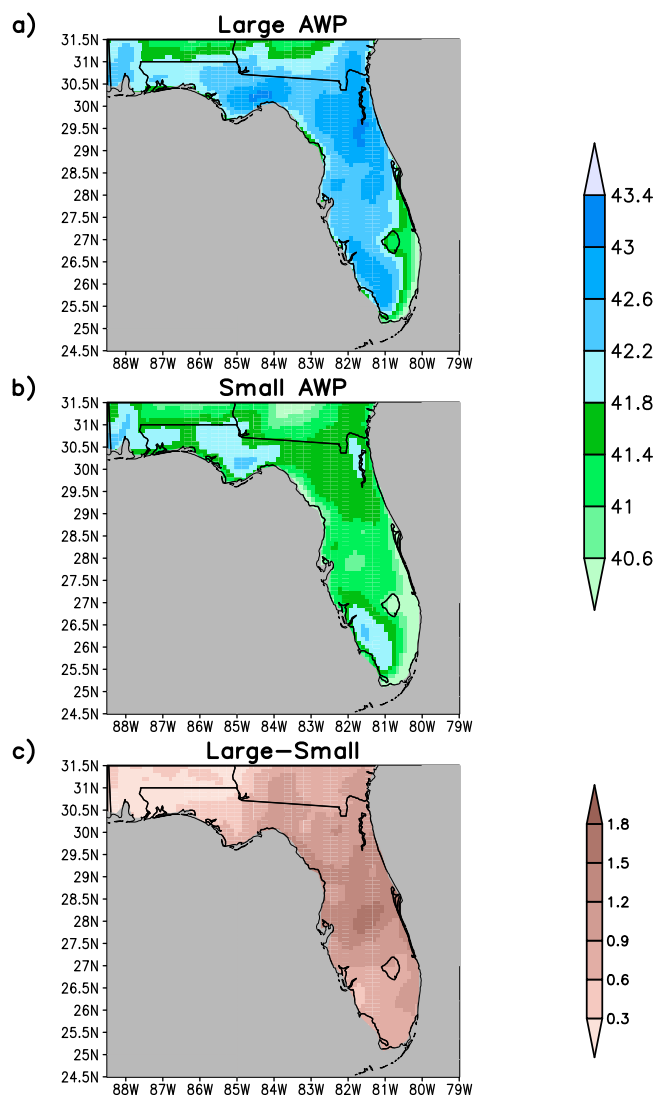


Figure 14. The JJA composite mean 16:00 EST JJA precipitable water computed for (a) large AWP years, (b) small AWP years, and (c) the difference of Figures 14a and 14b. The units are in kg m^{-2} .

vection along the northwestern coast of Florida become weaker than in the small AWP years. This is best illustrated in the schematic shown in Figure 12. The moisture budget calculation revealed that this reduction in sea breeze precipitation in large AWP years is accompanied with increase in the moisture content of the atmospheric column.

[22] The sea breeze in South Florida is complicated with the convergence of double sea breeze fronts from the Atlantic and Gulf coasts. Furthermore, the signal of the AWP variations on rainfall in South Florida is relatively weak. Therefore the conclusions of this study apply exclusively to the panhandle coast of Florida.

[23] **Acknowledgments.** We acknowledge the resources of the Computational and Information Systems Laboratory of NCAR to obtain some of the observational data sets used for verification in this study. This research

is supported by the NOAA grant NA07OAR4310221, USDA CDC grant 5U01EH000421, and contract G10AC00149, from the United States Geological Survey. T.J.S. III was supported by the USGS project, “La Florida: A Land of Flowers along a Latitude of Deserts” from the National Climate Change and Wildlife Science Center. The paper’s contents are solely the responsibility of the authors and do not necessarily represent the views of the USGS, USDA, CDC, or NOAA. We also acknowledge the support of the Florida State University high-performance computing center, where all the computations in the paper were conducted.

References

- Anthes, R. A. (1978), The height of the planetary boundary layer and the production of circulation in a sea breeze model, *J. Atmos. Sci.*, *35*, 1231–1239, doi:10.1175/1520-0469(1978)035<1231:THOTPB>2.0.CO;2.
- Blanchard, D. O., and R. E. Lopez (1985), Spatial patterns of convection in South Florida, *Mon. Weather Rev.*, *113*, 1282–1299, doi:10.1175/1520-0493(1985)113<1282:SPOCIS>2.0.CO;2.
- Chan, S., V. Misra, and H. Smith (2011), A modeling study of the interaction between the Atlantic warm pool, the tropical Atlantic easterlies, and the Lesser Antilles, *J. Geophys. Res.*, *116*, D00Q02, doi:10.1029/2010JD015260.
- Chou, M.-D., and K. T. Lee (1996), Parameterizations for the absorption of solar radiation by water vapor and ozone, *J. Atmos. Sci.*, *53*, 1203–1208, doi:10.1175/1520-0469(1996)053<1203:PFTAOS>2.0.CO;2.
- Chou, M.-D., and M. J. Suarez (1994), An efficient thermal infrared radiation parameterization for use in General Circulation Models, *NASA Tech. Rep. Ser. Global Mod. Data Assimilation*, *3*, 85 pp.
- Ek, M. B., K. E. Mitchell, Y. Lin, E. Rogers, P. Grunmann, V. Koren, G. Gayno, and J. D. Tarpley (2003), Implementation of Noah land surface model advances in the National Centers for Environmental Prediction operational mesoscale Eta model, *J. Geophys. Res.*, *108*(D22), 8851, doi:10.1029/2002JD003296.
- Higgins, R. W., W. Shi, E. Yarosh, and R. Joyce (2000), *Improved United States Precipitation Quality Control System and Analysis*, NCEP/Clim. Predict. Cent. Atlas 7, 40 pp., Natl. Oceanic and Atmos. Admin, Camp Springs, Md.
- Hong, S. Y., and H. L. Pan (1996), Nonlocal boundary layer vertical diffusion in a medium-range forecast model, *Mon. Weather Rev.*, *124*, 2322–2339, doi:10.1175/1520-0493(1996)124<2322:NBLVDI>2.0.CO;2.
- Hoskins, B. J., and B. Wang (2005), Large-scale atmospheric dynamics, in *The Asian Monsoon*, edited by B. Wang, pp. 357–415, Springer, New York.
- Juang, H. H., and M. Kanamitsu (1994), The NMC nested regional spectral model, *Mon. Weather Rev.*, *122*, 3–26, doi:10.1175/1520-0493(1994)122<0003:TNNRSM>2.0.CO;2.
- Kanamaru, H., and M. Kanamitsu (2007), Scale-selective bias correction in a downscaling of global analysis using a regional model, *Mon. Weather Rev.*, *135*, 334–350.
- Kanamitsu, M., W. Ebisuzaki, J. Woollen, S.-K. Yang, J. J. Hnilo, M. Fiorino, and G. L. Potter (2002), NCEP-DOE AMIP-II reanalysis (R-2), *Bull. Am. Meteorol. Soc.*, *83*, 1631–1643, doi:10.1175/BAMS-83-11-1631.
- Lim, Y.-K., L. B. Stefanova, S. C. Chan, S. D. Schubert, and J. J. O’Brien (2010), High-resolution subtropical summer precipitation derived from dynamical downscaling of the NCEP/DOE reanalysis: How much small-scale information is added by a regional model?, *Clim. Dyn.*, doi:10.1007/s00382-010-0891-2, in press.
- Lin, Y., and K. E. Mitchell (2005), The NCEP stage II/IV hourly precipitation analyses: Development and applications, paper 1.2 presented at 19th Conference on Hydrology, Am. Meteorol. Soc., San Diego, Calif., 9–13 Jan.
- Loveland, T. R., J. W. Merchant, B. C. Reed, J. F. Brown, D. O. Ohlen, P. Olson, and J. Hutchinson (1995), Seasonal land cover regions of the United States, *Ann. Assoc. Am. Geogr.*, *85*, 339–355.
- Misra, V., S. Chan, R. Wu, and E. Chassignet (2009), Air-sea interaction over the Atlantic warm pool in the NCEP CFS, *Geophys. Res. Lett.*, *36*, L15702, doi:10.1029/2009GL038737.
- Nicholls, M. E., R. A. Pielke, and W. R. Cotton (1991), A two-dimensional numerical investigation of the interaction between sea breezes and deep convection over the Florida peninsula, *Mon. Weather Rev.*, *119*, 298–323, doi:10.1175/1520-0493(1991)119<0298:ATDNIO>2.0.CO;2.
- Rodwell, M. J., and B. J. Hoskins (2001), Subtropical anticyclones and summer monsoons, *J. Clim.*, *14*, 3192–3211, doi:10.1175/1520-0442(2001)014<3192:SAASM>2.0.CO;2.

- Slingo, J. M. (1987), The development and verification of a cloud prediction scheme for the ECMWF model, *Q. J. R. Meteorol. Soc.*, *113*, 899–927.
- Smith, T. M., R. W. Reynolds, T. C. Peterson, and J. Lawrimore (2008), Improvements to NOAA's historical merged land-ocean surface temperature analysis (1880–2006), *J. Clim.*, *21*, 2283–2296, doi:10.1175/2007JCLI2100.1.
- Wang, C., and D. B. Enfield (2001), The tropical Western Hemisphere warm pool, *Geophys. Res. Lett.*, *28*, 1635–1638, doi:10.1029/2000GL011763.
- Wang, C., and D. B. Enfield (2003), A further study of the tropical Western Hemisphere warm pool, *J. Clim.*, *16*, 1476–1493, doi:10.1175/1520-0442-16.10.1476.
- Wang, C., D. B. Enfield, S.-K. Lee, and C. W. Landsea (2006), Influences of the Atlantic warm pool on the Western Hemisphere summer rainfall and Atlantic hurricanes, *J. Clim.*, *19*, 3011–3028.
- Wang, C., S.-K. Lee, and D. B. Enfield (2007), Impact of the Atlantic warm pool on the summer climate of the Western Hemisphere, *J. Clim.*, *20*, 5021–5040.
-
- S. Chan, J. J. O'Brien, and L. Stefanova, Center for Ocean-Atmospheric Prediction Studies, Florida State University, Tallahassee, FL 32306, USA.
- V. Misra and L. Moeller, Department of Earth, Ocean and Atmospheric Science, Florida State University, Tallahassee, FL 32306, USA. (vmisra@fsu.edu)
- N. Plant, St. Petersburg Coastal and Marine Science Center, U. S. Geological Survey, 600 Fourth St. S., St. Petersburg, FL 33701, USA.
- T. J. Smith III, Southeast Ecological Science Center, U. S. Geological Survey, 600 Fourth St. S., St. Petersburg, FL 33701, USA.